
Check for updates

developed [
ERO1.0, however it uses massive para
and thus allows simulating a significantly larger number of particles. Moreover, it is capable of simulating complex wall geometries of large toroidal devices including ITER. ERO2.0 was already used for the simulation of the Be erosion and transport in the JET ITER-like wall [21]. In the present study we use the ERO2.0 capability of handling complex surface geometries to reproduce a rough surface impact on erosion conducting the simulations with necessary level of detail on a micro- or nano-scale. In future this should allow improving the ITER modelling, however most probably using the multiscale approach, because typical ERO surface mesh size for JET or ITER is on the cm scale.

This study is focused on molybdenum (Mo) which is one of the materials used in ITER (for instance for mirrors, where roughness should not be larger than 1 nm [22]) and is a component of reduced-activation ferritic/martensitic (RAFM) steel considered as a PFC for future fusion devices [38]. In this contribution we implement the effect of surface roughness into the ERO2.0 code. Unlike in [21], where smooth tokamak PFC surfaces were assumed, we consider an extremely small simulation volume (1–2 μm^3), however in exchange use the computational power to treat the rough surface in full detail on the nanometer scale. Our aim is to investigate the influence of different types of surface roughness (both regular and irregular) on the effective sputtering yield and angular distribution of sputtered atoms, as well as evolution of the rough surface under the plasma irradiation. The predictive modelling is aimed to assist in on-going preparation of experiments at the PSI-2 linear plasma device with samples of pre-defined roughness [23–24] which are going to utilize several measurement techniques like Quartz-Micro Balance (QMB) [25], mass loss, optical emission spectroscopy and scanning electron microscopy (SEM) [26].

Here we focus on the case of perpendicular and nearly mono-energetic incidence of plasma ions on the surface (characteristic for PSI-2). In case of the glancing incidence ($\sim 87^\circ$ with the surface normal) characteristic for toroidal devises additional effects are coming into play (e.g. shadowing of surface structures [8], energy distribution of incident particles [27]). Considering these effects is out of the scope of the present study.

2. Incorporation of rough surface into ERO2.0

To use the code on the micro-/nano- scale several modifications have been introduced including various types of the regular structures well-imaginable for rough surfaces and a fractal-based irregular surface (see Fig. 1). An algorithm for the surface evolution during the plasma

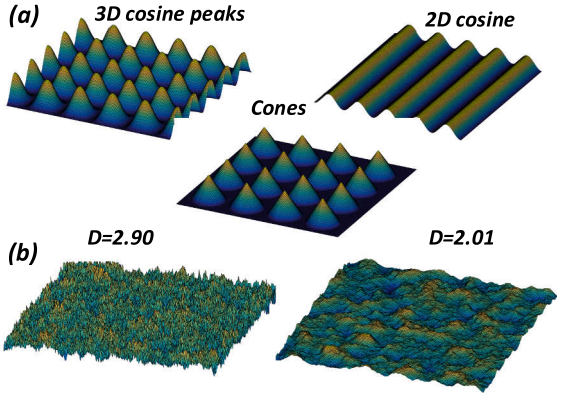

Fig. 1. Surfaces used for ERO2.0. a) Various regular general shapes, defined by the formulae; b) randomly generated surface defined with the fractal dimension D_{fract}.

assume
study [33] and use sputtering yields
functions for the SDTrimSP calculations proposed by Eckstein [40].

The ERO2.0 rough surface consists of smooth surface cells. The angle between the normal to the surface and the magnetic field influences the amount of material sputtered from this cell (sputtering yield is dependent on the ion impact angle) and the angular distribution of the sputtered atoms. Superposition of contributions from all the surface cells determines the resulting average values of the sputtering yield and the angular distribution of sputtered particles for the rough surface. In this study, a surface area of 4 μm^2 with 2.5×10^5 surface cells is simulated. Periodic boundaries are employed to represent a larger scale surfaces and to avoid artifacts due to the simulation volume boundaries.

2.1. Surface shapes implemented into ERO2.0

Several examples of surface structure shapes which are implemented into ERO2.0 are shown in Fig. 1. General surface shapes defined by a formula, as well as randomly-generated topographies (defined by e.g. the fractal dimension D_{fract}) can be created. The stochastic surfaces with certain D_{fract} value are created using the Fourier concept (power spectral density) [28]. Furthermore, the output of the atomic force microscope (AFM) [8] can be used as an input for ERO2.0. AFM is envisaged for interpretation of the surface roughness experiments planned at the PSI-2 facility. Two principally different types of surface are in the focus of this work (though more are investigated): regular cosine peaks and randomly-formed surfaces defined by a fractal dimension D_{fract}.

The surface with cosine peaks is defined with the generic formula:

$$z = h\cos^n\left(\frac{\pi}{w}x\right)\sin^n\left(\frac{\pi}{w}y\right) \tag{2.1.1}$$

Here $\boldsymbol{h}$ is the maximum height of the peaks, $\boldsymbol{n}$ is an even integer number defining the sharpness of the peaks and $\boldsymbol{w}$ is the distance between two neighbouring valleys. One of the main advantages of this surface is a wide range of structures that can be represented with this formula by varying $\boldsymbol{h}$, $\boldsymbol{n}$ and $\boldsymbol{w}$ – from shallow hills to the dense needles. Several examples of this constructed surface used as the test cases in this contribution are presented in Fig. 2. As shown below, the aspect ratio $\boldsymbol{h/w}$ and peak sharpness $\boldsymbol{n}$ are the key parameters for the modelling.

The randomly-generated surface with fractal dimension D_{fract} and the average height of the peaks $\boldsymbol{h}$ is presented in Fig. 1b for $D_{fract} = 2.01$ and $D_{fract} = 2.90$. This stochastic topography is characteristic to the irregular surface morphology, for instance naturally-formed during the plasma irradiation.

2.2. Sheath electric field near the rough surface

Rough surface interaction with the plasma can be strongly affected by the sheath electric field near the surface. Relation between the Debye length, the incident ions gyro-radius and the size of the surface structures determine whether the morphology structures have an effect on the local electric field [8,29]. For example, shape of the potential drop differs significantly for “valleys” in comparison to the “peaks” and depends on the width of the “valley” according to [39].

Analytical formulae for the sheath electric field value, including the effect of applied bias voltage and ion movement before hitting the surface, were proposed in ref. [27] for the smooth surface and were used in standalone preliminary simulations to produce the effective yields. Now these formulae have been incorporated directly into the

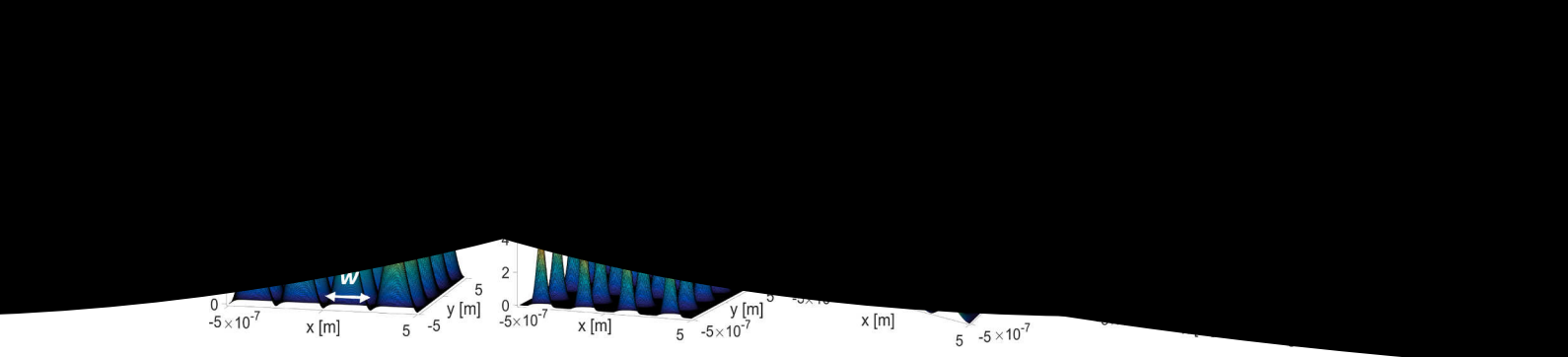

Fig. 2. Surface shapes for the considered test case (3D cosine peaks): aspect ratio ***h/w*** and the sharpness (power ***n*** in (1)) of the peaks are varied.

ERO2.0. They are applied for the rough surface in two boundary cases: when the sheath thickness is much smaller or much larger than the structures on the surface [8]. In the first case the sheath follows the shape of the surface which then can be at every point treated as locally-smooth. In the second case the sheath becomes much larger than the surface structures and is not affected by the roughness any more. All intermediate cases (when surface structure scale is comparable to the sheath depth) demand PIC-simulations to define the electric field distribution near the surface. First PIC simulations with the SPICE3 code [30] showed that this range is from $h_{\text{struct}}/R_{\text{Debye}} = 4$ to $h_{\text{struct}}/R_{\text{Debye}} = 434$ (which corresponds to $h_{\text{struct}}/R_{\text{Larmor}} = 1$). Those limits were determined from observing the profile of the electric field E in the perpendicular to the surface direction in one of the valleys. Outside of this range the E-field profile deviation from the one for the smooth surface can be neglected.

Direct measurements of plasma parameters (plasma density n_e, temperature T_e, flux) in the very vicinity of the target in the PSI-2 linear plasma device are not available at the moment. Therefore the one-dimensional (1D) PIC simulation code BIT1 [31] was applied for the modelling of the full volume of the PSI-2 facility. The distribution of plasma parameters along the main axis of the facility was obtained. As soon as the code is 1D, no radial distribution of plasma parameters was considered. First modelling results show that for D plasma the value of the Debye length near the target surface reaches 40 μm, while the maximum size of the roughness will not exceed 1 μm. Therefore, we can assert that for the considered experimental case the sheath electric field is not affected by the surface roughness. Moreover, due to the negative target bias ($U_b = -250$ V) we assume perpendicular incidence of plasma ions to the general horizontal of the target surface (despite we take into account different local incident angles due to the rough surface, see below). Thus, tracking of individual incident plasma ions is not necessary in this study. In order to save the computational time they are treated as a mono-energetic beam with the energy $\boldsymbol{E = eU_b - eU_{plasma}}$, where U_{plasma} is the plasma potential.

2.3. Angular distribution of sputtered particles

Angular distribution of sputtered particles is crucial for the modelling of rough surface sputtering, because it determines the amount of sputtered material re-deposited on the neighbouring structures. In previous ERO applications cosine ($f(\theta) = \cos(\theta)$) and "butterfly" ($f(\theta) = A\cos^n(\theta) - B\cos^m(\theta)$, with *A,B,n,m* dependent on the incident energy, masses of target and incident species, e.g. $f(\theta) = 4.0\cos^{1.9}(\theta) - 3.5\cos^{3.2}(\theta)$ in this study) [32] polar angle (θ) distributions were assumed as a first approximation (exact choice cosine/butterfly dependent on the irradiation conditions). The azimuthal angle φ was assumed to be homogeneously distributed between 0 and 2π. It was observed experimentally [33] and shown with the modelling [34] that, for large oblique angles of incidence, sputtered particles tend to move along the projection of the incident particles velocity direction on the surface (Fig. 3b). The significance of this effect for the modelling of surfaces with complex topographies is high due to the large fraction of oblique areas.

The influence of incidence angle on the resulting angular distribution of sputtered particles was implemented into ERO2.0. The local coordinate system for a single surface cell is shown in the Fig. 3a. To take into account the above described "new" angular distribution, for which the azimuthal angle distribution peaks in the specular direction, a cosine distribution of φ was assumed as a first approximation. The polar angle θ distribution stayed the same as in previous ERO modelling efforts [32], i.e. "butterfly"-like (see Fig. 3c). In order to reflect the fact that such changes in the angular distribution happen only for large oblique angles [34], the cosine φ-distribution was applied only for incident angles larger than $\pi/4$, otherwise it was assumed as before to be isotropic. The $\pi/4$ value was chosen as the first approximation. The exact value of angle at which the collision cascade results in inhomogeneity of φ distribution depends multiple factors, such as the angle, energy of incidence particles, mass ratio of the incident and target species [33,34]. As a result, for the oblique local (with the normal to the surface) angles of incidence, sputtered particles are released preferably in the direction of incidence projected on the surface (Fig. 3d). In this work, simulation results with both "new" (with "butterfly"-shaped for θ and cosine for φ) and "old" ("butterfly"-shaped for θ, isotropic for φ) angular distributions cases are shown.

Also using direct results of the SDTrimSP5.7 [35] calculations (energy, angular distributions and the sputtering yield) is currently available in the code. This demands conducting the SDTrimSP simulation for every energy-angle combination and using the output of these runs as an input for ERO2.0. For the tests described in this contribution we use the analytical model discussed above.

2.4. Surface evolution during the irradiation

Both sputtering and re-deposition influence surface topography evolution during the plasma irradiation. In order to model this evolution an algorithm for surface changes on every time step was implemented in ERO2.0.

The *XY* mesh, parallel to the target surface, stays fixed, while the *Z*-coordinates of the surface vertices are varied. The simulation domain is adapted for the possible surface changes, so that all the vertices are staying inside of it. First the sputtered/redeposited thickness is calculated for every surface cell – negative for net erosion, positive for net deposition. This thickness is calculated according to the following formula:

$$\Delta z = Y \cdot \Gamma \cdot dt \cdot 1/n_{atomic} \tag{2.4.1}$$

Here Y is the sputtering yield, Γ is the incident ion flux [m^{-2} s^{-1}], dt is the simulation time step, n_{atomic} is the target atomic density [m^{-3}].

The centroid of each surface cell is then shifted along the normal of this surface cell together with the plane corresponding to this cell. New intersections of this plane with the *XY* mesh are calculated and averaged over 4 neighbouring cells at every *XY* mesh node. Then new *Z* coordinate of the centroid and the nominal angle are recalculated. To avoid numerical errors, two correction procedures described in [36] and extended to the 3D surface are applied: averaging of the each vertex's *Z* position over the 8 neighbouring vertices and correction of excessive changes of *Z*-coordinate leading to the reversal of the surface cell slope.

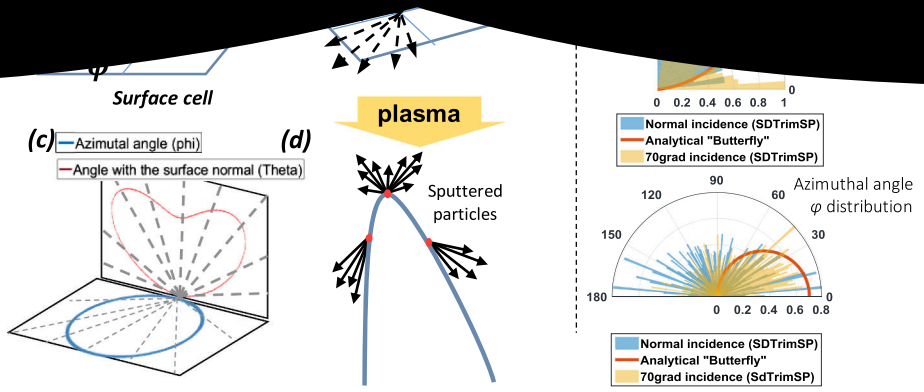

various local incidence [illegible]
"new" analytical azimuthal/polar angular distribution with the direct SDTrimSP calculations for D->Mo, E = 500 eV, α = 0°, 70°.

3. Predictive ERO2.0 modelling of the PSI-2 surface roughness experiments

The plasma parameters used in the test cases were those of the PSI-2 facility with a typical D plasma: magnetic field $B = 0.1$T, flux $\Gamma = 1.4 \times 10^{21}$ m^{-2} s^{-1}, plasma density $n_e = 4.7 \times 10^{11}$ cm^{-3}, plasma temperature $T_e = 8.5$ eV bias voltage $U_b = -250$ V. The Mo ionization length in PSI-2 is of the order of 1 cm, therefore the tracked sputtered particles were neutral and possible uncertainties in the description of the sheath electric field $\boldsymbol{E}$ (the absolute value and direction of $\boldsymbol{E}$ near the rough surface) do not play any role. All the presented runs were conducted on the supercomputer JURECA [41].

3.1. Effective sputtering yield and angular distribution of sputtered particles

The effective sputtering yield $Y_{\text{eff\_rough}}$ of the rough surface is defined as the amount of sputtered target atoms, which also escape the rough surface (means, not deposited at the neighbouring surface structures), per incident particle. In the Fig. 4a the ratio between the effective sputtering yield $Y_{\text{eff\_rough}}$ of the rough surface and that of the smooth one (Y_{smooth}) is shown as a function of the surface structure aspect ratio ($\boldsymbol{h/w}$ from (1)). Results are presented for two types of angular distribution – the "new" one with the φ distribution and the "old", only the "butterfly" for θ. Resulting polar angular distributions of the sputtered particles for the rough surface for the cases from Fig. 2 are shown in the Fig. 5. The polar angular distribution for the smooth surface is shown for comparison. No effective azimuthal distribution is shown, because for this type of surface it is homogenous from 0 to 2π, due to the surface regularity, conical symmetry of the peaks and incidence of plasma ions being perpendicular to the surface. The influence of the surface fractal dimension D_{fract} on the effective sputtering yield is presented in Fig. 4b.

One can see in Fig. 4a that the effective sputtering yield is decreasing with the surface structure aspect ratio rising. Also the case with $Y_{\text{eff\_rough}}/Y_{\text{smooth}} > 1$ can be observed for the very low aspect ratio values. This is due to the fact that for low surface structures' aspect ratios sputtered particles are still not collected by the neighbouring peaks, but already the local sputtering yield for some surface cells becomes larger due to the locally shallower than normal incidence. Also one can notice that sharper structures ($n = 10$) tend to let more particles out than the blunt ones ($n = 2$). At the same time, one can see in the Fig. 5 that the preferential polar angle of sputtering shifts to the normal direction with the increase of the surface structure aspect ratio (collimation effect). The additional peak of the distributions at large angles for topographies with $n = 2$ is due to the spherical tops of the peaks. Particles starting there are not deposited on the neighbouring peaks, at that surface cells in those areas are inclined enough to influence the angular distribution of these particles. When in this simulation cosine peaks are replaced with the cones of the same proportions, this feature decreases significantly or vanishes.

Both effects (decrease of $Y_{\text{eff\_rough}}$ and collimation of the polar angular distribution) have been observed experimentally at the PISCES-B

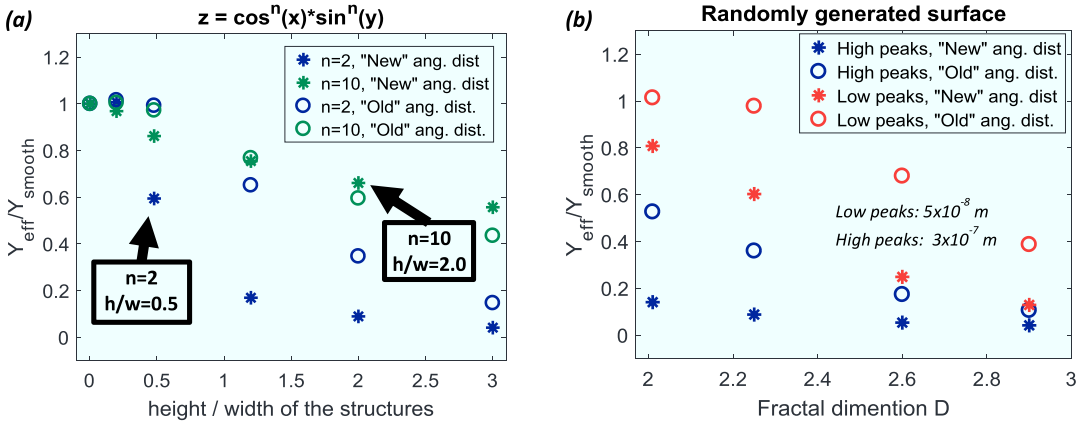

Fig. 4. Ratio of the effective sputtering yield of the rough surface to the sputtering yields of the smooth surface (Eckstein data [40] are used for the smooth cases) for the case of a) surface with 3D cosine peaks as a function of the surface structures aspect ratio; b) randomly generated surface as a function of the surface fractal dimension D_{fract} changing in the range $D_{\text{fract}} = 2.01$–2.90.

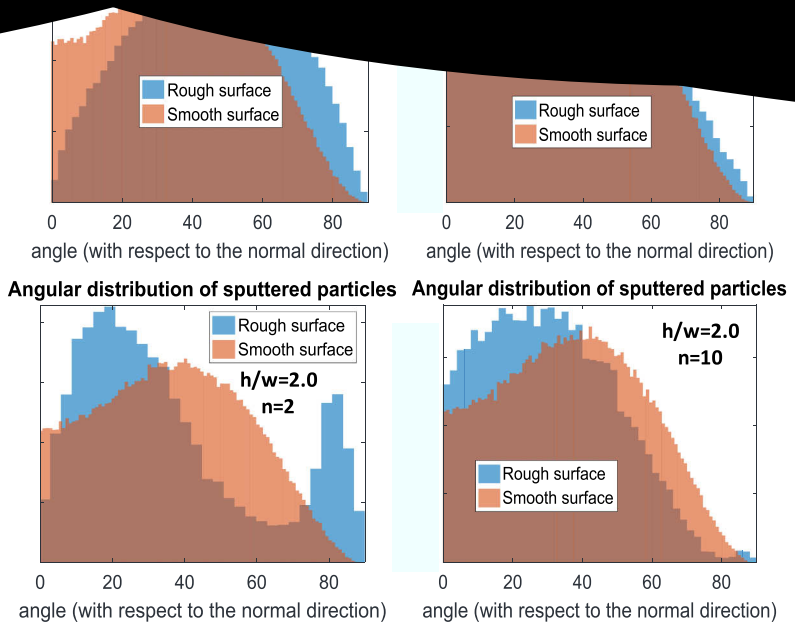

Fig. 5. Effective angular distribution of sputtered particles of the surface with 3D cosine peaks for the cases from the Fig. 3.

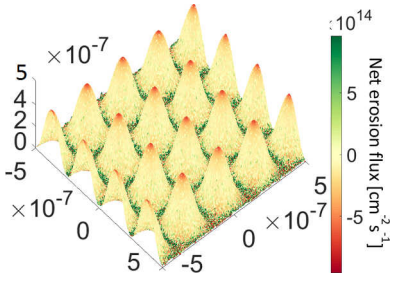

Fig. 6. Initial shape of the surface with cosine peaks. Net erosion in the beginning of the irradiation. Height of the peaks: 5×10^{-7} m, $h/w = 2.0$, $n = 2$.

linear plasma device for the Be irradiation by D [9]. Both increase of the decay length of impurity penetration in the plasma (it is larger when more particles are starting with angles close to the surface normal) and decrease of the spectroscopy signal were observed for the developed needle-like structures.

In the Fig. 4b one can notice that the increase of the fractal dimension D_{fract} also leads to the decrease of the $Y_{\text{eff\_rough}}$. The correction for the angular distribution of sputtered particles implemented in this study results in a further reduction of $Y_{\text{eff\_rough}}$.

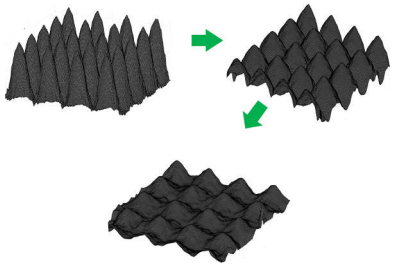

Fig. 7. Surface evolution during the plasma irradiation. Corresponding fluences and irradiation times are given in the Table 1.

3.2. Surface evolution under plasma irradiation

Surface evolution during the plasma irradiation was simulated for the PSI-2 facility conditions (see above). The initial shape of the surface as well as the net erosion/deposition areas are shown in Fig. 6. The peak aspect ratio is $\boldsymbol{h/w} = 2.0$ and $\boldsymbol{n} = 2$, see (1). The initial absolute height of the peaks is $\boldsymbol{h} = 5 \times 10^{-7}$ m. In the Fig. 6 one can see that due to the strong re-deposition of the sputtered particles on the neighbouring peaks, the net erosion occurs only at the tops. At the same time, the strongest re-deposition is located in the valleys.

The time evolution of the surface topography is shown in Fig. 7. One can notice the flattening of the surface, due to sputtering of the peaks and re-deposition in the valleys shown in Fig. 6, which leads (as was shown in Fig. 4) to the increase of $Y_{\text{eff\_rough}}$ during the irradiation. Moreover, the valleys are not eroded until the peaks are significantly eroded (in ≈6 h 30 min, see Table 1). This result serves as a guidance for choosing the plasma parameters and irradiation times for the PSI-2 roughness experiments.

Further transport of the sputtered particles escaping the surface is not considered in this study, however planned for interpretation of experiments in PSI-2. Sputtered particles are ionized in the plasma and certain fraction of them comes back to the surface causing self-sputtering of the target. This effect can be taken into account by combining

Table 1
Values of irradiation times and fluence are corresponding to the steps of the surface evolution shown in Fig. 6.

#	Time of irradiation [h, min]	Fluence [m-2]	Surface minimum coordinate [m]	Peak height [m]
0	0	0	0	5×10^{-7}
1	6.5 min	5.6×10^{23}	0	4.5×10^{-7}
2	2 h 40 min	1.4×10^{25}	0	2.3×10^{-7}
3	6 h 30 min	3.2×10^{25}	$\approx -1 \times 10^{-7}$	1.0×10^{-7}

Conclusions

In the frame of this work the effect of surface roughness was implemented into the 3D Monte-Carlo PSI and plasma impurity transport code ERO2.0. The influence of the surface roughness on the average sputtering yield, re-deposition and angular distribution of the sputtered Mo, in the conditions characteristic for the linear plasma device PSI-2, was investigated for several constructed roughness types (both regular and stochastic). The results were parameterized as a function of the surface structures aspect ratio or fractal dimension respectively. It was shown that the considered roughness types lead to the decrease of erosion and collimation of the resulting angular distribution of Mo atoms escaping the surface. For example for the certain regular structures, the effective sputtering yield decreases by a factor of 6 with the increase of the surface structures aspect ratio $\boldsymbol{h/w}$ from 0.1 to 3.0. Similarly, the effective sputtering yield decreases up to factor 4 for irregular structures on stochastic surface with the change of the surface fractal dimensionality from $D_{\text{fract}} = 2.01$ to $D_{\text{fract}} = 2.90$. Therefore, more fine surface morphology seems to suppress the physical sputtering.

Several improvements were necessary for treating the sputtering on the slopes of the fine structures. For instance, accounting for azimuthal angular distribution of sputtered species due to the oblique plasma ions incidence is responsible for the general $Y_{\text{eff\_rough}}$ decrease. In the frame of the actual approach, preferential re-deposition in the "valleys" and erosion at the "hills" are leading to the flattening of the surface. This means that additional effects should be included into the model to describe those experimental cases in which the structures are observed to grow.

This work provides an insight useful for planning of the upcoming experiments at PSI-2 device aimed at studying of the surface roughness effect. It can also be of high value for other ERO applications to erosion modelling at plasma devices with PFCs that are not smooth due to manufacturing as well as due to the plasma operation.

Acknowledgements

This work has been carried out within the framework of the EUROfusion Consortium and has received funding from the Euratom research and training programme 2014–2018 under grant agreement no 633053. This work was supported by Czech Science Foundation project GA16-14228S and by the IT4Innovations Centre of Excellence project (CZ.1.05/1.1.00/02.0070). The views and opinions expressed herein do not necessarily reflect those of the European Commission. The authors gratefully acknowledge the computing time granted

[1] G.F. [illegible]
[2] M.J. Rubel, et al., Fusion Eng. Des. 81 [illegible]
[3] Y. Hirooka, et al., Nucl. Instrum. Methods Phys. Res. Sect. B 23 [illegible]
[4] S. Kajita, et al., Nucl. Fusion 49 (9) (2009) 095005.
[5] M.J. Baldwin, et al., Nucl. Fusion 48 (3) (2008) 035001.
[6] A. Kreter, et al., Plasma Phys. Control. Fusion 50 (9) (2008) 095008.
[7] A. Hakola, et al., Phys. Scr. T159 (2014) 014027.
[8] K. Schmid, M. Mayer, C. Adelhelm, et al., Nucl. Fusion 50 (2010) 105004.
[9] R.P. Doerner, et al., Phys. Scr. T159 (2014) 014040.
[10] T. Abe, et al., J. Nucl. Sci. Technol. 15 (7) (1978) 471–475.
[11] A. Terra, et al., Micro-structured tungsten; an advanced plasma-facing material, International Conference on Plasma Surface Interactions in Controlled Fusion Devices, Princeton University, NJ, 2018.
[12] J.N. Brooks, D.N. Ruzic, Modeling and analysis of surface roughness effects on sputtering, reflection, and sputtered particle transport. No. CONF-900505–10, Argonne National Lab. (1990).
[13] S. Quan, et al., Contrib. Plasma Phys. 57 (8) (2017) 329–335.
[14] D. Shuyu, et al., Nucl. Fusion 54 (12) (2014) 123015.
[15] A. Kreter, et al., Fusion Sci. Technol. 68 (1) (2015) 8–14.
[16] A. Kirschner, et al., Nucl. Fusion 40 (5) (2000) 989.
[17] A. Kirschner, et al., Phys. Scr. T138 (2009) 014011.
[18] A. Eksaeva, et al., Phys. Scr. T170 (2017) 014051.
[19] D. Borodin, et al., Phys. Scr. T128 (2007) 127.
[20] D. Borodin, et al., Contrib. Plasma Phys. 50 (3208) (2010) 432–438 5.
[21] J. Romazanov, et al., Phys. Scr. T170 (2017) 014018.
[22] A. Litnovsky, et al., Nucl. Fusion 47 (8) (2007) 833.
[23] E. Vassallo, et al., Thin Solid Films 558 (2014) 189–193.
[24] E. Vassallo, et al., Surf. Coat. Technol. 214 (2013) 59–62.
[25] H.G. Esser, et al., Fusion Eng. Des. 66 (2003) 855–860.
[26] J.I. Goldstein, et al., Scanning Electron Microscopy and X-ray Microanalysis, Springer, 2017.
[27] I. Borodkina, et al., Nucl. Mater. Energy 12 (2017) 341–345.
[28] J.B. Florindo, et al., Physica A 391 (20) (2012) 4909–4922.
[29] R.H. Cohen, D.D. Ryutov, Contrib. Plasma Phys. 40 (4) (2000) 456–470 3208.
[30] M. Komm, et al., Plasma Phys. Control. Fusion 55 (2) (2013) 025006.
[31] D. Tskhakaya, et al., Parallel, distributed and network-based processing (PDP), 2010 18th Euromicro International Conference on, IEEE, 2010.
[32] A. Eksaeva, et al., Nucl. Mater. Energy 12 (2017) 253–260.
[33] G. Betz, et al., Int. J. Mass Spectrom. Ion Process. 140 (1) (1994) 1–110.
[34] J.P. Biersack, et al., Appl. Phys. A 34 (2) (1984) 73–94.
[35] A. Mutzke, et al., Nano-scale modification of 2D surface structures exposed to 6 keV carbon ions: Experiment and modeling, Nuclear Instruments and Methods in Physics Research Section B: Beam Interactions with Materials and Atoms 269 (6) (2011) 582–589.
[36] T. Ishitani, et al., J. Mater. Sci. 9 (3) (1974) 505–508.
[37] D. Borodin, et al., Improved ERO modelling of beryllium erosion at ITER upper first wall panel using JET ILW and PISCES-B experience, International Conference on Plasma Surface Interactions in Controlled Fusion Devices, Princeton University, NJ, 2018.
[38] E. Lucon, et al., Fusion Eng. Des. 81 (8–14) (2006) 917–923.
[39] W. Hu, et al., Nucl. Mater. Energy 12 (2017) 313–317.
[40] W. Eckstein, Top. Appl. Phys. 110 (2007) 33–187.
[41] Jülich Supercomputing Centre, JURECA: Modular supercomputer at Jülich Supercomputing Centre, Journal of large-scale research facilities 4 (2018) A132 http://dx.doi.org/10.17815/jlsrf-4-121-1.